

Charged-particle spectroscopy for diagnosing shock pR and strength in NIF implosions

A. B. Zylstra, J. A. Frenje, F. H. Séguin, M. J. Rosenberg, H. G. Rinderknecht et al.

Citation: *Rev. Sci. Instrum.* **83**, 10D901 (2012); doi: 10.1063/1.4729672

View online: <http://dx.doi.org/10.1063/1.4729672>

View Table of Contents: <http://rsi.aip.org/resource/1/RSINAK/v83/i10>

Published by the [American Institute of Physics](#).

Related Articles

Performance of a short “magnetic bottle” electron spectrometer

Rev. Sci. Instrum. **83**, 063106 (2012)

Velocity-map imaging at low extraction fields

Rev. Sci. Instrum. **83**, 063101 (2012)

Theory of collisional electron spectroscopy for gas analysis

J. Appl. Phys. **111**, 114503 (2012)

The geometric factor of electrostatic plasma analyzers: A case study from the Fast Plasma Investigation for the Magnetospheric Multiscale mission

Rev. Sci. Instrum. **83**, 033303 (2012)

Design and operation of the wide angular-range chopper spectrometer ARCS at the Spallation Neutron Source

Rev. Sci. Instrum. **83**, 015114 (2012)

Additional information on Rev. Sci. Instrum.

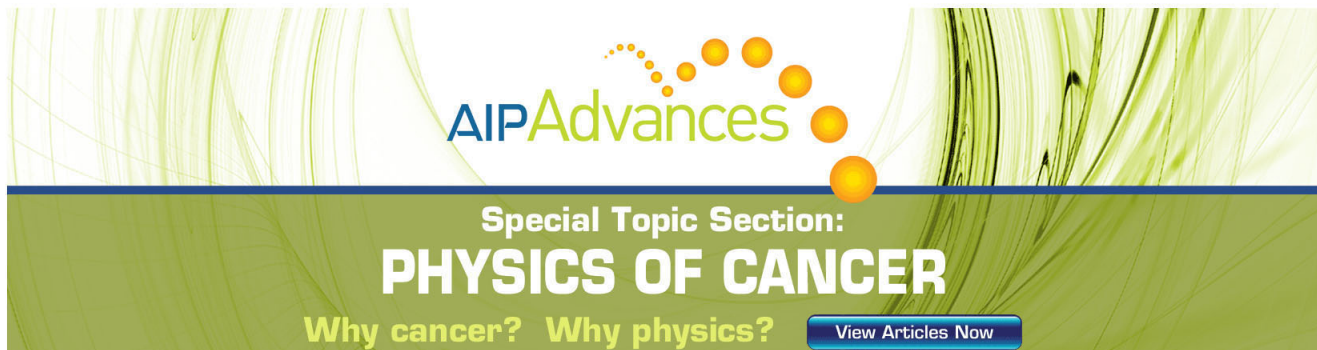
Journal Homepage: <http://rsi.aip.org>

Journal Information: http://rsi.aip.org/about/about_the_journal

Top downloads: http://rsi.aip.org/features/most_downloaded

Information for Authors: <http://rsi.aip.org/authors>

ADVERTISEMENT



AIPAdvances

Special Topic Section:
PHYSICS OF CANCER

Why cancer? Why physics? [View Articles Now](#)

Charged-particle spectroscopy for diagnosing shock ρR and strength in NIF implosions^{a)}

A. B. Zylstra,^{1,b)} J. A. Frenje,¹ F. H. Séguin,¹ M. J. Rosenberg,¹ H. G. Rinderknecht,¹ M. Gatu Johnson,¹ D. T. Casey,¹ N. Sinenian,¹ M. J.-E. Manuel,¹ C. J. Waugh,¹ H. W. Sio,¹ C. K. Li,¹ R. D. Petrasso,¹ S. Friedrich,² K. Knittel,² R. Bionta,² M. McKernan,² D. Callahan,² G. W. Collins,² E. Dewald,² T. Döppner,² M. J. Edwards,² S. Glenzer,² D. G. Hicks,² O. L. Landen,² R. London,² A. Mackinnon,² N. Meezan,² R. R. Prasad,² J. Ralph,² M. Richardson,² J. R. Rygg,² S. Sepke,² S. Weber,² R. Zacharias,² E. Moses,² J. Kilkenny,³ A. Nikroo,³ T. C. Sangster,⁴ V. Glebov,⁴ C. Stoeckl,⁴ R. Olson,⁵ R. J. Leeper,⁵ J. Kline,⁶ G. Kyrala,⁶ and D. Wilson⁶

¹Plasma Science and Fusion Center, Massachusetts Institute of Technology, Cambridge, Massachusetts 02139, USA

²Lawrence Livermore National Laboratory, Livermore, California 94550, USA

³General Atomics, San Diego, California 92186, USA

⁴Laboratory for Laser Energetics, University of Rochester, Rochester, New York 14623, USA

⁵Sandia National Laboratory, Albuquerque, New Mexico 87185, USA

⁶Los Alamos National Laboratory, Los Alamos, New Mexico 87545, USA

(Presented 8 May 2012; received 7 May 2012; accepted 29 May 2012; published online 19 June 2012)

The compact Wedge Range Filter (WRF) proton spectrometer was developed for OMEGA and transferred to the National Ignition Facility (NIF) as a National Ignition Campaign diagnostic. The WRF measures the spectrum of protons from D-³He reactions in tuning-campaign implosions containing D and ³He gas; in this work we report on the first proton spectroscopy measurement on the NIF using WRFs. The energy downshift of the 14.7-MeV proton is directly related to the total ρR through the plasma stopping power. Additionally, the shock proton yield is measured, which is a metric of the final merged shock strength. © 2012 American Institute of Physics. [<http://dx.doi.org/10.1063/1.4729672>]

I. INTRODUCTION

The National Ignition Facility (NIF) is a 1.8 MJ 192 beam ignition-scale laser for inertial confinement fusion (ICF) experiments.¹ ICF requires proper assembly of the fusion fuel for ignition and burn.^{2,3} In particular, the cold DT (deuterium and tritium) fuel must reach a high enough areal density (ρR), which is primarily measured by the magnetic recoil spectrometer⁴⁻⁷ and neutron time of flight (nTOF) spectrometers.⁸

Non-cryogenic experiments are conducted as part of the NIF tuning campaign,^{9,10} such as implosions to correct asymmetries in the radiation drive by measuring the compressed shape^{11,12} with x-ray self-emission imaging, and similar experiments¹³ to measure the implosion velocity and remaining mass, and thus the implosion kinetic energy, with x-ray radiography. In these capsules, the cryogenic fuel layer is replaced with a surrogate mass of plastic (CH) and the capsules are filled with a D₂ + ³He gas fuel mixture, which produces the fusion reaction D + ³He → ⁴He(3.6 MeV) + p(14.7 MeV) among others.

Of particular interest is the 14.7 MeV proton from D³He fusion. By measuring the proton spectrum, the energy lost while traversing the implosion is known, and thus the line-

integrated mass and total ρR are determined. This technique has been used extensively on the OMEGA laser facility¹⁴ to study implosion physics.^{15,16} Several Wedge Range Filter (WRF) spectrometers^{17,18} have been implemented at the OMEGA and NIF.

In ICF, a series of shocks are driven into the capsule by a specifically shaped laser pulse. The shock timing is tuned so that the subsequent shocks catch up to the first, coalesce, then collapse in the core before the peak compression of the capsule. This gives two distinct nuclear production times, hereafter referred to as “shock” and “compression”.^{16,17,19}

Measurements of proton spectra during the shape and velocity tuning campaigns give important observables which are used to study the effects of implosion tuning; for example these data shed light on the in-flight mass profile and final merged shock strength, which impacts the hot-spot adiabat and shell deceleration. Additionally, these data could be systematically compared to radiation-hydrodynamics simulations in LASNEX (Ref. 20) and HYDRA (Ref. 21) as a benchmark of those codes.

II. STOPPING POWER CALCULATIONS

To infer ρR from the energy loss we must calculate the stopping power for an energetic proton in a plasma. We use the Li-Petrasso stopping power model.²² The simplest model assumes that all ρR comes from a spherical shell of carbon-hydrogen (CH) plasma. At shock (compression) burn the con-

^{a)}Contributed paper, published as part of the Proceedings of the 19th Topical Conference on High-Temperature Plasma Diagnostics, Monterey, California, May 2012.

^{b)}Electronic mail: zylstra@mit.edu.

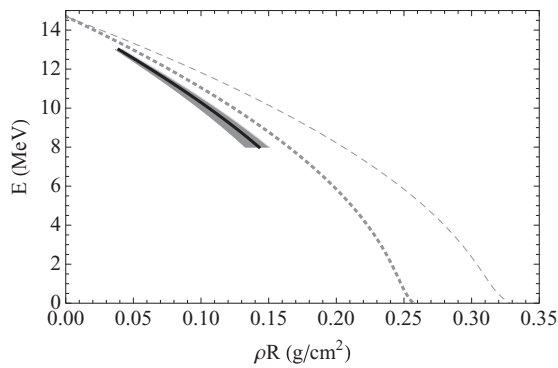


FIG. 1. $D^3\text{He}$ proton energy versus total ρR , calculated using the Li-Petrasso²² dE/dx for various ρR models: in a carbon-hydrogen (CH) plasma for the compression phase (dashed gray) and the shock phase (dotted gray). The black curve represents a HYDRA-derived model with error bars represented by the gray shaded region.

vergence is low (high) and the shell is best represented by $\rho = 10(100) \text{ g/cm}^3$. In both cases the temperature is assumed $T_e = T_i = 0.5 \text{ keV}$. The measured proton energy versus implosion ρR is calculated using this model and shown in Fig. 1.

In reality, the in-flight ρR is composed of the nuclear fuel, remaining ablator material, and ablated mass. The fuel and ablated mass have much higher T_e and lower ρ than the cold shell, and therefore lower stopping power.²² This is particularly important during the shock phase, when the remaining shell can have only $\sim 50\%$ of the total ρR , resulting in lower ρR for a given downshift compared to the spherical shell model (Fig. 1). Using a radiation-hydrodynamics simulation from HYDRA, we construct a model where mass-averaged ρ and T_e are taken for each of the three regions (fuel, shell, ablated mass) from the simulation. The shell convergence is then artificially varied to generate a curve of downshifted proton energy versus ρR . The model uncertainty is 50% error bars in ρ and T_e represented by the gray shaded region.

We assume that this stopping model accurately reflects capsule conditions within $\pm 50\%$ in ρ and T_e (shaded region, Fig. 1). This error is added in quadrature with the precision of the WRF to give an absolute error in ρR .

III. EXPERIMENTAL SETUP

Figure 2 shows the NIF experimental setup. WRFs are fielded on Diagnostic Instrument Manipulators (DIMs), in particular on DIMs (0,0) and (90,78) [chamber coordinates (θ, ϕ) , where $\theta = 0$ is vertically up]. One to two WRFs are fielded on each DIM; future capability will allow four detectors on DIM (90,78). On DIM (0,0) the WRFs have a clear line of sight to Target Chamber Center. The DIM (90,78) WRFs look through the hohlraum. Depending on the experimental campaign the hohlraum wall at this line of sight is up to $64 \mu\text{m}$ of Au or depleted uranium (DU) and up to $74 \mu\text{m}$ of Al. The uncertainty in material thickness is $\pm 1 \mu\text{m}$ Au/DU and $\pm 3 \mu\text{m}$ Al. For some hohlraums one line of sight from DIM (90,78) is obscured by the thick Al thermo-mechanical band; these data are not used. All proton spectra are corrected for the hohlraum-induced energy downshift using cold-matter

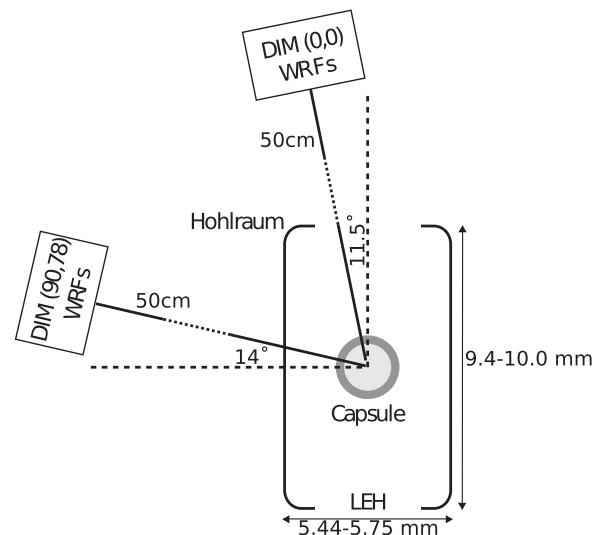


FIG. 2. Schematic of the experimental setup at NIF. The hohlraum is shown with capsule inside. The DIM (0,0) WRFs view the implosion through the laser entrance hole (LEH) at an angle of 11.5° to the hohlraum axis, while the DIM (90,78) WRFs view through the hohlraum wall at an angle of 14° to the equator.

stopping powers,²³ which is a valid approximation according to integrated hydrodynamics calculations.

The capsule fill is generally 30:70 atomic D: ^3He . The total laser energy used was between 1 MJ and 1.6 MJ, with varying pulse shapes due to ongoing ignition tuning. The hohlraum material was Au or DU; the hohlraum geometry was varied between 5.44 mm (“544”) and 5.75 mm (“575”) outer diameter.

IV. DATA

Figure 3 shows proton spectra measured on NIF shape tuning shot N110208, a 544 Au hohlraum, shot with 1.3 MJ total laser energy. The areal density measured on the pole ($\rho R = 65 \pm 10 \text{ mg/cm}^2$) and equator ($\rho R = 68 \pm 8 \text{ mg/cm}^2$) are equivalent within error bars. Therefore these data are consistent with a symmetric in-flight implosion during the shock burn. However, simulations indicate $\rho R = 77\text{--}85 \text{ mg/cm}^2$ at shock flash, suggesting that the implosion is at a larger radius (lower convergence) during the shock burn than predicted. This is also apparent as a difference in energy downshift, making it unlikely that the discrepancy can be explained by systematic ρR model uncertainties. Between 8–10 MeV on the equator we see additional proton production associated with the start of compression burn; these protons are downshifted more than the shock protons meaning they were produced later in time at higher ρR .

The shock proton yield measured on the equator [$Y_p = (2.43 \pm 0.44) \times 10^8$] is much higher than the polar measurement [$Y_p = (1.48 \pm 0.35) \times 10^7$]. This is due to strong transverse magnetic or electric fields at the LEH which deflect protons measured at DIM (0,0) but do not affect equatorial measurements (see Fig. 2); time variation in the fields causes loss of compression protons on the pole. This is consistent with previous experiments^{24–26} at OMEGA. Using the equatorial measurement only, we compare to post-shot simulations that

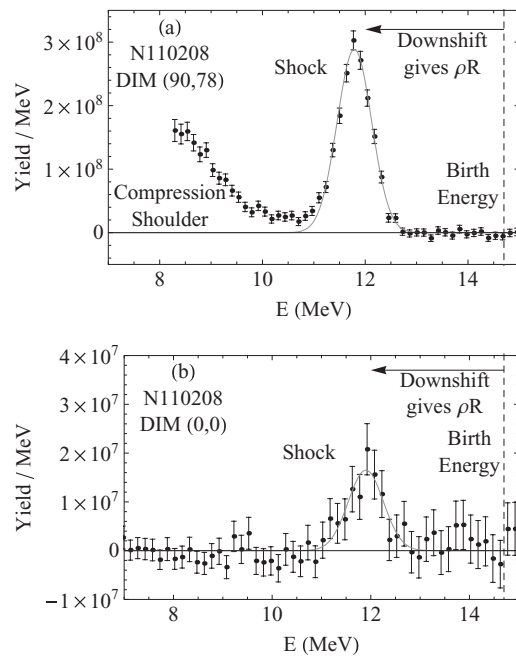


FIG. 3. D^3He proton spectrum measured on NIF shot N110208 (1.3 MJ shape tuning shot with a 544 Au hohlraum) on DIM (90,78) (a) and DIM (0,0) (b). The downshift from the birth energy at 14.7 MeV (dashed line) gives the ρR . Gaussian fits to the shock peak are shown in gray. On the equator, $Y_p = (2.43 \pm 0.44) \times 10^8$ and $E = 11.79 \pm 0.14$ MeV, corrected for the hohlraum downshift, corresponding to $\rho R = 68 \pm 8$ mg/cm². On the pole, we measured a yield of $Y_p = (1.48 \pm 0.35) \times 10^7$ and $E = 11.90 \pm 0.26$ MeV corresponding to $\rho R = 65 \pm 10$ mg/cm².

have $Y_p = 2.9 \times 10^9$ for this implosion, giving a yield over clean of $\approx 10\%$.

V. CONCLUSIONS

We report the first proton spectra measured on the NIF in D^3He gas-filled indirect-drive implosions using the compact WRF spectrometer. The spectral shape is used to infer the shock proton yield, a measure of shock strength, and the in-flight ρR at shock flash time. Compared to hydrodynamics simulations, the shock proton yield is lower than modeled by a factor of 10 and the in-flight ρR at shock flash is lower, implying less shell convergence by shock flash. The WRFs have recorded high-quality data on over 60 NIF shots, including more than 45 indirect-drive D^3He gas-filled implosions.

Extensive future work is planned for the large WRF data set at NIF: implementing the particle time of flight (pTOF) diagnostic²⁷ to measure the shock bang time, developing an implosion model describing the complete proton spectrum, using a Guderley self-similar imploding shock solution^{19,28} to infer the final merged shock strength from the proton yield, studying the observed field-induced proton deficits through

the LEH, and using occasional observed asymmetries between the WRF lines of sight will be systematically studied to infer the implosion shape, particularly for P_2 modes.

ACKNOWLEDGMENTS

The authors thank the engineering, operations, and technical staff at NIF, Laboratory for Laser Energetics (LLE), and Massachusetts Institute of Technology for their support. This work was done in part for A. B. Zylstra's Ph.D. thesis and was supported in part by the (U.S.) Department of Energy (DOE) (DE-FG52-09NA29553), Lawrence Livermore National Laboratory (LLNL) (B580243), LLE (414090-G), the Fusion Science Center at the University of Rochester (415023-G), and the National Laser Users Facility (DE-NA0000877). This work was performed under the auspices of the DOE by LLNL under Contract No. DE-AC52-07NA27344. A. B. Zylstra is supported by the DOE National Nuclear Security Administration Stewardship Science Graduate Fellowship (DE-FC52-08NA28752).

¹G. Miller, E. Moses, and C. Wuest, *Nucl. Fusion* **44**, S228 (2004).

²J. Nuckolls, L. Wood, A. Thiessen, and G. Zimmerman, *Nature (London)* **239**, 139 (1972).

³J. Lindl, *Phys. Plasmas* **2**, 3933 (1995).

⁴J. Frenje *et al.*, *Rev. Sci. Instrum.* **72**, 854 (2001).

⁵J. Frenje *et al.*, *Rev. Sci. Instrum.* **79**, 10E502 (2008).

⁶J. Frenje *et al.*, *Phys. Plasmas* **17**, 056311 (2010).

⁷D. T. Casey, *Diagnosing Inertial Confinement Fusion Implosions at OMEGA and the NIF Using Novel Neutron Spectrometry* (MIT, 2012).

⁸V. Glebov *et al.*, *Rev. Sci. Instrum.* **77**, 10E715 (2006).

⁹O. Landen *et al.*, *Phys. Plasmas* **17**, 056301 (2010).

¹⁰S. Glenzer *et al.*, *Science* **327**, 1228 (2010).

¹¹G. Kyrala *et al.*, *Phys. Plasmas* **18**, 056307 (2011).

¹²G. Kyrala *et al.*, *Rev. Sci. Instrum.* **81**, 10E316 (2010).

¹³D. Hicks, B. Spears, D. Braun, R. Olson, C. Sorce, P. Celliers, G. Collins, and O. Landen, *Phys. Plasmas* **17**, 102703 (2010).

¹⁴T. Boehly *et al.*, *Opt. Commun.* **133**, 495 (1997).

¹⁵R. Petrasso *et al.*, *Phys. Rev. Lett.* **90**, 95002 (2003).

¹⁶J. Frenje *et al.*, *Phys. Plasmas* **11**, 2798 (2004).

¹⁷F. Séguin *et al.*, *Rev. Sci. Instrum.* **74**, 975 (2003).

¹⁸F. Séguin *et al.*, "Advances in compact proton spectrometers for inertial-confinement-fusion and plasma nuclear science," *Rev. Sci. Instrum.* (these proceedings).

¹⁹J. R. Rygg, *Shock Convergence and Mix Dynamics in Inertial Confinement Fusion* (MIT, 2006).

²⁰G. Zimmerman and W. Kruer, *Controlled Fusion* **2**, 51 (1975).

²¹M. Marinak, G. Kerbel, N. Gentile, O. Jones, D. Munro, S. Pollaine, T. Dittrich, and S. Haan, *Phys. Plasmas* **8**, 2275 (2001).

²²C. Li and R. Petrasso, *Phys. Rev. Lett.* **70**, 3059 (1993).

²³J. Ziegler, J. Biersack, and U. Littmark, *The Stopping and Range of Ions in Matter* (Pergamon, New York, 1985).

²⁴C. Li *et al.*, *Phys. Rev. Lett.* **102**, 205001 (2009).

²⁵C. Li *et al.*, *Science* **327**, 1231 (2010).

²⁶F. Philippe *et al.*, *Phys. Rev. Lett.* **104**, 35004 (2010).

²⁷H. Rinderknecht *et al.*, "A novel particle Time Of Flight (pTOF) diagnostic for measurements of shock- and compression-bang times in D^3He and DT implosions at the NIF," *Rev. Sci. Instrum.* (these proceedings).

²⁸G. Guderley, *Luftfahrtforsch* **19**, 302 (1942).